Electronic Supplementary Material (ESI) for Soft Matter.
This journal is © The Royal Society of Chemistry 2018

Overview: The Janus-nature of molecular CO_2 in charge adjustment at wet surfaces

Peter Vogel,[a♦] Muhammad Nawaz Qaisrani,[b♦] Mattis Rasenat,[a] Johannes Lützenkirchen,[c] Marialore Sulpizi,[d] David Beyer,[e] Christian Holm,[e] and Thomas Palberg*[a]

[a]Institute of Physics, Johannes Gutenberg University, Mainz, Germany.

[b]Institute of Physics and Institute of Micro- and Nanotechnologies, Technische Universität, Ilmenau, Germany

[c]Institute for Nuclear Waste Disposal (INE), Karlsruhe Institute of Technology (KIT), Karlsruhe, Germany

[d]Department of Physics, Ruhr Universität Bochum, Bochum, Germany

[e]Institute of Computational Physics (ICP), University Stuttgart, Stuttgart, Germany.

♦both authors contributed equally

* Corresponding author: palberg@uni-mainz.de

Conditioning

For the interested reader, we here give a short summary on the development of conditioning procedures employing ion exchange resins. By far the most common technique for deionization is simply the introduction of ion exchange resin IEX into a (precleaned) sample contained in a (sealed) cell. The exchange process is believed to be completed when particle ordering appears after a period of several weeks [1]. This allowed to study phase behavior and crystal formation and shear melting in aqueous charged sphere suspensions at extremely low volume fractions of $< 10^{-5}$ [2, 3], whereas, in non-agitated, and in particular in badly sealed, samples, a vertical density gradient may evolve and even lead to the separation of differently ordered regions: crystals at the cell bottom, a middle region of lower density and fluid order and a supernatant depleted phase. This stratification, however, is absent in samples sealed using screw caps with gas-tight Teflon$^{(R)}$ septa to avoid gradient induced artifacts [4]. Repeating gentle stirring of the sample further accelerates deionization considerably. This observation was later used to develop gas tight conditioning circuits, where the suspension is continuously pumped through an ion exchange column [5]. A sketch of the set-up is shown in Fig. S1. Leakage of ions from the container walls is avoided using PMMA-based vessels. Care has to be taken, to use gas tight tubings and fittings. Again, Teflon$^{(R)}$ is a good choice. Valves, fittings and connections are meanwhile commercially available. To exclude contamination by airborne CO_2, the reservoir is kept under an inert gas atmosphere. After assembly, a known volume of pre-cleaned suspension is added and slowly cycled through the system. Using the scheme in Fig.1, for the first time allowed monitoring the ensuing deionization process in situ. Both light transmission and conductivity are monitored in flow-trough cells. The system was considered ion-free after reaching a minimum conductivity. For crystallizing samples, one may alternatively use the crystallite size obtained after shear melting. This quantity is even more sensitive to residual contaminations and evolves monotonously with progressing deionization. Typical deionization times are around half an hour for 100ml of sample.

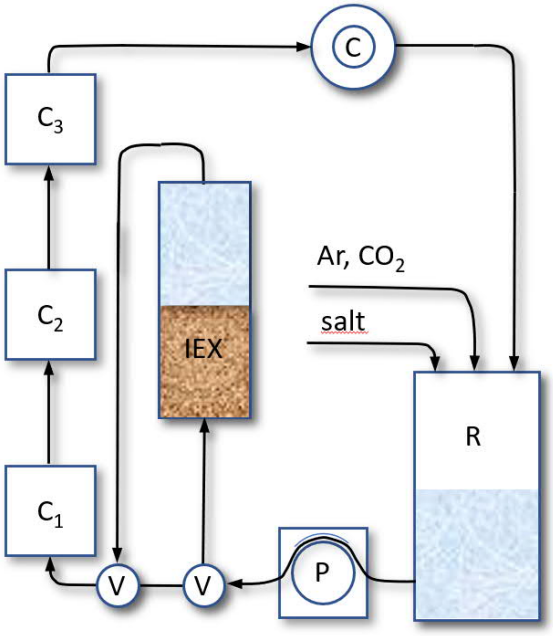

Figure S1: Conditioning circuit as used in the present experiments. R: reservoir under Ar Atmosphere with inlets for CO_2 and salt solution, P: peristaltic pump, IEX: ion exchange column, C_1, C_2, C_3, ...: optical flow through cells, C: conductometric cell. All components are connected by gas tight tubings, with flow direction indicated as arrows. After thorough deionization the IEX can be bypassed using the valves (V). Then, salt solution can be added to the reservoir under an inert gas atmosphere and its concentration monitored via conductivity. Note that this flexible set-up allows the integration of a large number of parallel optical experiments under identical, well controlled conditions. In the standard configuration of the present paper, we use photometric pH determination, turbidity measurements and laser Doppler velocimetry. It is, however easily adapted to other experimental needs.

Precise adjustment of finite small ion concentrations, however, required the development of a reliable conductivity model. Schaefer was the first to point out the linear dependence of conductivity on particle concentration and, using the specific conductivity of protons, related the former to an effective particle charge [6]. Deggelmann later suggested to improve that approach by additionally considering experimentally determined particle mobilities [7]. The decisive step towards reliable monitoring of the concentrations of added small ions, however was taken in the model of independent ion migration by Hessinger, where for the first time all ionic species were accounted for [8]. That model, moreover, also allowed to describe the exchange processes between differently mobile ionic species (depicted e.g. in Fig. 3 (b) of the main text), as well as reactions occurring upon titration. Later, it was also successfully applied to the temperature dependence of suspension conductivities [9] and the conductivity of mixtures [10].

With the implementation of a precise in situ salt concentration control, the full flexibility of the scheme sketched in Fig. S1 became exploitable. Now, several experiments connected by the tubing system could be used to investigate different properties of the suspension in parallel at identical conditions [11].

Integral, reference beam configuration, Super Heterodyne Laser Doppler Velocimetry

Heterodyning, also known as laser Doppler velocimetry (LDV), is a well-established technique to measure velocities in fluids and colloidal suspensions [12]. It found widespread and commercial application in electro-kinetics of colloidal systems, where the measured particle mobility $\mu = v / E$ is related to its charge state by the standard electrokinetic model and its extensions [13, 14, 15, 16]. LDV is typically performed in closed cells of rectangular geometry, as sketched in Fig. S2(a). In such cells, the electro-osmotic slip at the (negatively) charged wall and the incompressibility of the solvent lead to a pronounced velocity profile within the cell. Fig. S2(b) shows the solvent profile u(x, y=0) at mid-cell height as dotted blue parabola Along the cell wall, the solvent drifts with v_{eo} towards the negative electrode (upper red arrow). It flows back in the center. The full profile $u_S(x,y)$ can be numerically calculated as a function of cell height h and cell width d [Fig. S2 (c)] [17]; an analytic solution is known at mid cell-height, h =0 [18, 19]. A stationary level is defined by $u_S(x,y) = 0$ [dashed lines in Figs. S2 (b) and (c)]. The velocity profile of charged tracer particles (solid blue line) is determined by the solvent profile and the phoretic velocity v_{ep} of the particles against the solvent, $v_p(x,y) = u_S(x,y) + v_{ep}$ (lower red arrow).

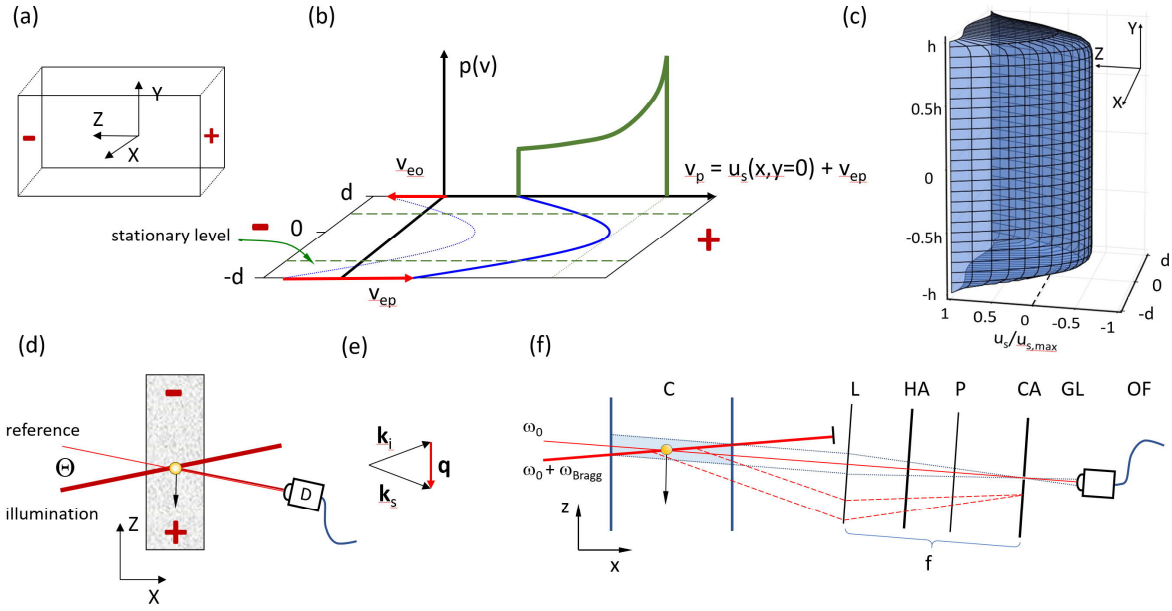

Figure S2: Optical set-up. (a) Principal cell geometry with coordinate directions and a pair of electrodes indicated. (b) Mid-cell height solvent (dashed blue) and particle velocity (solid blue) profile and resulting normalized particle velocity distribution [p(v), solid green]. (c) Numerically determined electro-osmotic solvent flow in a cell of K = h/d = 20. Electrode positions are assumed to be as sketched in (a) and (b). Solvent velocities are normalized to the electro-osmotic velocity us,max = veo. Vertical y-axis: normalized cell height h; x-axis: normalized cell depth d. (d) Top view sketch of the light scattering principle in reference beam configuration. At the detector (D), light scattered off the illumination beam by a negatively charged particle moving towards the anode is mixed with non-scattered light of the reference beam. (e) The scattering vector $\vec{q} = \vec{k}_s - \vec{k}_i$ is colinear to the particle velocity. (f). Top view of the superheterodyne detection scheme cut in the scattering plane (x-z). In the cell (C), the frequency shifted illumination beam (thick red line) is crossed by the reference beam (thin red line) under an angle $\Theta = 8°$ in air. The illumination beam is stopped by a beam stopper. Light

leaving the cell parallel to the reference beam is focused by the lens (L, f = 50mm) into the focal plane, where a circular aperture (CA) is placed. The position and width of CA defines the direction of the scattering vector q and the q-resolution Δq, respectively. The minimum opening is chosen to about 1mm in order let a sufficient amount of reference beam light pass. A grin lens (GL, diameter 4mm) mounted on an optical fiber (OF) is aligned collinear with the reference beam and guides the collected light to the detector. The distance between CA and GL defines the diameter of the detection volume (light blue). It is chosen as to contain the complete illuminating beam crossing the cell. Light originating outside the detection volume as well as light leaving the cell in directions not sufficiently parallel to the reference beam (e.g. dashed red lines) is blocked. Light scattered out of the x-z plane is optionally rejected by a horizontally mounted slit aperture (HA). A polarizer (P) assures V/V detection. If L and CA are removed, the q-resolution is defined by solely the acceptance angle of the grin lens and the maximum detection volume by the acceptance angle and the GL diameter. It typically is larger than with CA and L and is slightly conical.

v_{ep} is directly measurable at the stationary level or inferred from the center of mass of the velocity distribution p(v) determined by LDV. A principal scheme of LDV in reference beam configuration is given in Fig. S2 (d). Two laser beams cross in the cell under an angle Θ. At the detector (D), light scattered off moving particles is superimposed with non-scattered light from a reference beam. This creates a beat which is frequency analyzed using Fast Fourier Transformation (FFT, not shown). Moving particles create a spectral signal at $\omega_D = q \bullet v$ in the Doppler- or power-spectrum. Here, the scattering vector $q = k_i - k_s$ is defined in Fig. S2 (e), with k_i and k_s being the wave vectors of the illuminating and the singly scattered beam, respectively. Its magnitude is given by $q = (4\pi\nu)/\lambda \sin(\Theta/2)$ with ν being the suspension refractive index.

To measure both wall-slip v_{eo} and v_{ep} over a wide range of particle concentrations several challenges have to be overcome. First, the desired heterodyne spectral contribution, which contains the desired velocity-information, has to be separated from the superimposing homodyne contribution (stemming from mixing light scattered off different particles) and unwanted low frequency contributions from mechanical vibrations or electronic noise). Adapting ideas from radio-physics, Schätzel et al. were the first to introduce an additional frequency difference ω_{Bragg} between the two beams [20]. In the resulting superheterodyne (SH) spectrum, the heterodyne contribution is shifted by ω_{Bragg} towards larger frequencies and can be readily isolated.

Second, to avoid tedious point-by-point measurements employing scans of the crossing point through the cell cross-section, we had combined SH-LDV with an integral measurement [19]. An additional benefit of this integral approach is an excellent ensemble averaging, which makes it readily applicable to nonergodic systems like colloidal glasses or polycrystalline solids [21]. Figure 1(f) shows the fibre-optic version used in [22]. In integral mode, the reference beam light can mix with light scattered in reference beam direction from all particles illuminated by the widened illumination beam along its path along the whole cell cross-section. Since these particles show a normalized velocity distribution, p(v) [c.f. Fig. S2 (b)], the Doppler spectra, $C_{shet}(\mathbf{q},\omega)$, display a corresponding normalized distribution of Doppler frequencies, $p(\omega_D)$. This can be accounted for by a convolution integral: [23]:

$$C_{shet}(\mathbf{q},\omega) = \int d\omega_D \; p(\omega_D) C^0_{shet}(\mathbf{q},\omega) \qquad \text{(S1)},$$

where for particles undergoing Brownian motion with an effective diffusion coefficient D_{eff} and directed motion with a constant and homogenous drift velocity v. the single particle spectrum $C^0_{shet}(\mathbf{q},\omega)$ reads:

$$C^0_{shet}(\mathbf{q},\omega) = \left[I_r + \left\langle I_1(\mathbf{q}) \right\rangle \right]^2 \delta(\omega) + \frac{\left\langle I_1^0(\mathbf{q}) \right\rangle^2}{\pi} \frac{2q^2 D_{eff}(q)}{\omega^2 + \left(2q^2 D_{eff}(q)\right)^2} + \frac{I_r \left\langle I_1(\mathbf{q}) \right\rangle}{\pi} \left[\frac{q^2 D_{eff}(q)}{\left(\omega + \left[\omega_B - \omega_D\right]\right)^2 + \left(q^2 D_{eff}(q)\right)^2} + \frac{q^2 D_{eff}(q)}{\left(\omega - \left[\omega_B - \omega_D\right]\right)^2 + \left(q^2 D_{eff}(q)\right)^2} \right]$$

(S2)

Here, I_r is the reference beam intensity. $\left\langle I_1(\mathbf{q}) \right\rangle = I_0 n b^2(0) P(q) S_M(q)$ is the time-averaged singly scattered intensity, with the constant I_0 comprising experimental boundary conditions like illumination intensity distance to the detector and polarization details. n is the particle number density, b^2 is the single particle forward scattering cross section, P(q) denotes the particle form factor, and $S_M(q)$ the measurable static structure factor [24, 25].

The integral SH-spectrum contains three contributions: a trivial constant term centered at zero frequency, a homodyne Lorentzian of width $2q^2D_{eff}$ which is also centered at the origin and independent of the particle drift motion, and two super-heterodyne Lorentzians of spectral width q^2D_{eff} symmetrically shifted away from the origin by both the Bragg frequency and the Doppler frequency. Therefore, further analysis needs to consider only the positive part of the spectrum in the vicinity of the Bragg frequency. For further details of the corresponding scattering theory, interested readers are referred to the ESI and to [22].

At elevated concentrations, colloidal systems may develop a pronounced fluid or even crystalline order which can be further modified by shear [26, 27]. Performing electrokinetic experiments inevitably shear the suspension with position dependent shear rates, which may lead to structural inhomogeneities [28]. As a consequence, $S_M(q)$ may vary across the cell cross-section and render Eqn. (2) useless. This third challenge is avoided in the set-up of Fig. 1(f) by using small scattering angles ($\Theta \approx 2°$-$8°$). At such small angles, scattering is dominated by incoherent contributions resulting e.g. from size dispersity [24]. This ensures detection of single particle rather than collective dynamics and facilitates measurements which are neither dependent on the overall suspension structure nor its homogeneiety. [28, 29]. A final difficulty at elevated concentrations is encountered by multiple scattering, which can become very massive. As discussed in the main text, an empirical correction may be applied during the fitting procedure [22].

A nice feature of Eqn. (S1) is its dependence on two independent parameters, v_{eo} and v_p. Therefore, the spectral shape obtained in experiments in a fluid phase can be interpreted in terms of three independent parameters yielding independent information on the electroosmotic mobility at the cell wall and the electrophoretic mobility of the tracers. Eqn. (S2) only introduces one additional (symmetric broadening) parameter, D_{eff}. In [30], we combined integral reference beam super heterodyne LDV with a custom-made sample cell featuring exchangeable side walls. This allowed for the first time the investigation of

surfaces beyond those of standard tracer particles and of the quartz wall present in our flow-through cells [31]. In the main text of this paper, we show measurements obtained on sapphire (0001) surfaces.

Notes and references

1 T. Okubo. Langmuir 10, 1695 – 1702 (1994). Giant colloidal single crystals of polystyrene and silica spheres in deionized suspensions.

2 D. J. W. Aastuen, N. A. Clark, L. K. Cotter, B. J. Ackerson, Phys. Rev. Lett. 57, 1733 (1986); 57, 2772 (1986) (E); Nucleation and Growth of Colloidal Crystals

3 T. Okubo, H. Fujita, Colloid Polym. Sci. 274, 368-374 (1996). Phase diagram of alloy crystal in the exhaustively deionized suspensions of binary mixtures of colloidal spheres

4 T. Palberg, M. Würth, Phys. Rev. Lett. 72, 786 (1994). Comment on Tata et al.:„Vapour-liquid condensation in charged colloidal suspensions

5 T. Palberg, W. Härtl, U. Wittig, H. Versmold, M. Würth, E. Simnacher, J. Phys. Chem. 96, 8180-8183 (1992). Continuous deionization of latex suspensions

6 D. W. Schaefer, J. Chem. Phys. 66, 3980 (1977). Colloidal Suspensions as soft core liquids

7 M. Deggelmann, T. Palberg, M. Hagenbüchle, E. E. Maier, R. Krause, C. Graf, R. Weber, J. Colloid Interf. Sci. 143, 318-326 (1991). Electrokinetic properties of aqueous suspensions of polystyrene spheres in the gas and liquidlike phase

8 D. Hessinger, M. Evers, T. Palberg, Phys. Rev. E 61, 5493-5506 (2000). Independent Ion Migration in Suspensions of Strongly Interacting Charged Colloidal Spheres

9 M. Medebach, R. Chuliá Jordán, H. Reiber, H.-J. Schöpe, R. Biehl, M. Evers, D. Hessinger, J. Olah, T. Palberg, E. Schönberger, P. Wette, J. Chem. Phys. 123, 104903 (2005). Drude type conductivity in charged sphere colloidal crystals: density and temperature dependence

10 P. Wette, H.-J. Schöpe, R. Biehl, T. Palberg, J. Chem. Phys. 114, 7556-7562 (2001). Conductivity of deionised two-component colloidal suspensions

11 P. Wette, H. J. Schöpe, J. Liu, T. Palberg, Prog. Colloid Polym. Sci. 123, 264-268 (2004). Characterization of colloidal solids

12 R. J. Adrian (Ed.), Selected papers on Laser Doppler velocimetry SPIE Milestone Series Vol. 78 1993.

13 R. W. O´Brien and L. R. White, J. Chem. Soc. Faraday Trans. II 74, 1607-1629 (1978). Electrophoretic mobility of a spherical colloidal particle

14 A. Delgado, F. González-Caballero, R. J. Hunter, L. K. Koopal, J. Lyklema, Pure Appl. Chem. 77, 1753–1805 (2005). Measurement and interpretation of electrokinetic phenomena

15 F. Carrique, F. J. Arroyo, A. V. Delgado, J. Colloid Interface Sci. 252, 126-137 (2002). Electrokinetics of concentrated suspensions of spherical colloidal particles with surface conductance, arbitrary zeta potential, and double-layer thickness in static electric fields

16 F. Carrique, E. Ruiz-Reina, R. Roa, F. J. Arroyo, Á. V. Delgado, J. Colloid Interface Sci. 455 46-54 (2015). General electrokinetic model for concentrated suspensions in aqueous

electrolyte solutions: Electrophoretic mobility and electrical conductivity in static electric fields

17 N. L. Burns, J. Colloid Interface Sci. 183, 249–259 (1996). Surface Characterization through Measurement of Electroosmosis at Flat Plates

18 S. Komagata, Researches Electrotech. Lab. Tokyo Comm. 348, 1-114 (1933).

19 T. Palberg, H. Versmold, (1989), J. Phys. Chem., 93, 5296-5301. Electrophoretic-electroosmotic light scattering

20 J. F. Miller, K. Schätzel, and B. Vincent, J. Colloid Interface Sci. 143, 532–554, (1991). The determination of very small electrophoretic mobilities in polar and nonpolar colloidal dispersions using phase analysis light scattering

21 T. Preis, R. Biehl, T. Palberg, Prog. Colloid Polym. Sci. 110, 129-133 (1998). Phase Transitions in colloidal dispersions flowing through a cylindrical tube

22 D. Botin, L. Marota Mapa, H. Schweinfurth, B. Sieber, C. Wittenberg, T. Palberg, J. Chem. Phys. 146, 204904 (2017). An Empirical Correction for Moderate Multiple Scattering in in Super-Heterodyne Light Scattering

23 T. Palberg, T. Köller, B. Sieber, H. Schweinfurth, H. Reiber, and G. Nägele. J. Phys.: Condens. Matter 24, 464109 (2012). Electro-kinetics of Charged-Sphere Suspensions Explored by Integral Low-Angle Super-Heterodyne Laser Doppler Velocimetry

24 G. Nägele, Phys. Reports 272, 215-372 (1996). Habil
On the dynamics and structure of charge-stabilized suspensions

25 J. K. G. Dhont, An introduction to the dynamics of colloids, Elsevier, Amsterdam 1996.

26 P. Wette, I. Klassen, D. Holland-Moritz, D. M. Herlach, H.J. Schöpe, N. Lorenz, H. Reiber, T. Palberg, S. V. Roth, J. Chem. Phys. 132, 131102 (2010). Communications: Complete description of re-entrant phase behaviour in a charge variable colloidal model system

27 B. J. Ackerson, N. A. Clark, Physica A 128, 221-249 (1983). Sheared colloidal suspensions

28 M. Medebach, T. Palberg, J. Chem. Phys. 119, 3360-3370 (2003). Phenomenology of Colloidal Crystal Electrophoresis

29 M. Medebach, L. Shapran, T. Palberg, Colloid Surfaces B 56, 210-219 (2007). Electrophoretic flow behaviour and mobility of colloidal fluids and crystals

30 D. Botin, J. Wenzel, R. Niu, T. Palberg, Soft Matter 14, 8191-8204 (2018). Colloidal electro-phoresis in the presence of symmetric and asymmetric electro-osmotic flow

31 P. Vogel. N. Möller, M. N. Qaisrani, B. Pravash, S. Weber H.-J. Butt, B. Liebchen, M. Sulpizi, T. Palberg, J. Am. Chem. Soc. 144, 21080–21087 (2022). Charging of dielectric surfaces in contact with aqueous electrolyte - the influence of CO_2